J|A|C|S ARTICLES

Published on Web 06/29/2010

Nano Building Blocks via Iodination of $[PhSiO_{1.5}]_n$, Forming $[p\text{-}I\text{-}C_6H_4SiO_{1.5}]_n$ (n = 8, 10, 12), and a New Route to High-Surface-Area, Thermally Stable, Microporous Materials via Thermal Elimination of I_2

M. F. Roll,[†] J. W. Kampf,[‡] Y. Kim,[‡] E. Yi,[§] and R. M. Laine*[,†,§]

Macromolecular Science and Engineering, Department of Chemistry, and Materials Science and Engineering, University of Michigan, Ann Arbor, Michigan 48109-2136

Received April 1, 2010; E-mail: talsdad@umich.edu

Abstract: We describe the synthesis and characterization of the homologous *p*-iodophenylsilsesquioxanes (SQs) $[p\text{-}I\text{-}C_6H_4SiO_{1.5}]_n$ (n = 8, 10, 12) via ICl-promoted iodination (−40 to −60 °C) with overall yields of 80−90% and >95% para selectivity following recrystallization. Characterization by NMR, FTIR, TGA, and single-crystal X-ray diffraction are reported and compared to data previously published for I_8OPS. Coincidentally, we report a new synthesis of the elusive pentagonal decaphenyl SQ (dPS) $[C_6H_4SiO_{1.5}]_{10}$ and its characterization by NMR and single-crystal X-ray studies. These unique macromolecules possess equivalent chemical functionality but varying symmetries (cubic, pentagonal, and D_{2d} dodecahedral), offering the potential to develop homologous series of functionalized star and dendrimer compounds with quite different core geometries and thereby providing the potential to greatly vary structure−property relationships in derivative compounds and nanocomposites made therefrom. We find that all three compounds decompose on heating to ∼400 °C/N_2 with loss of I_2 to form robust, microporous materials with BET surface areas of 500−700 m^2/g, pore volumes of 0.25−0.31 cm^3/g, average pore widths of 8 Å, and oxidative stabilities ≥500 °C and with solid-phase morphologies varying from crystalline to mostly amorphous, as indicated by powder XRD and SEM studies. These latter findings point to important symmetry effects relating directly to packing in the crystalline phase prior to thermolysis.

Introduction

The assembly of 2- and 3-D structures from molecular components or nanobuilding blocks (NBs) is of great current interest.[1−9] Altering the chemical reactivity of these NBs through synthetic means would presumably allow modulation of the coupling and interaction between the blocks in order to tailor global properties exactly at the finest length scales.[10]

Although there are numerous literature examples of molecules possessing high degrees of 2-D symmetry, only a smaller number of molecular classes possessing structure and functionality with high 3-D symmetry are known.[4−9] Cubic symmetry in 3-D and octa-functionality, such that each octant in Cartesian space contains one functional group, is particularly desirable to impart a high degree of functionality and facilitate assembly, with the proper choice of functionality.

However, having a family of molecules that provide multiple, high 3-D symmetries and a plethora of possible functional groups offers the opportunity to compare and contrast a wide variety of properties ranging from molecular packing and assembly[11−15] to electronic and photonic interactions between functional groups on the same molecule or in close-packed intermolecular structures.[16−20] It is of interest to investigate the relationship between the morphology of the final 3-D assembly with respect to the constituent nano building block. One might presume that the highest symmetry would impart the greatest degree of order after assembly.[1]

[†] Macromolecular Science and Engineering.
[‡] Department of Chemistry.
[§] Materials Science and Engineering.

(1) Detken, A.; Zimmermann, H.; Haeberlen, U.; Poupko, R.; Luz, Z. *J. Phys. Chem.* **1996**, *100*, 9598–9604.
(2) Hawker, C. J.; Wooley, K. L. *Science* **2005**, *309*, 1200–1205.
(3) Feynman, R. *J. Microelectromech. Syst.* **1992**, *1*, 60–66.
(4) Eaton, P. E.; Galoppini, E.; Gilardi, R. *J. Am. Chem. Soc.* **1994**, *116*, 7588–7596.
(5) Eaton, P. E.; Pramod, K.; Emrick, T.; Gilardi, R. *J. Am. Chem. Soc.* **1999**, *121*, 4111–4123.
(6) Reichert, V. R.; Mathias, L. J. *Macromolecules* **1994**, *27*, 7015–7023.
(7) Reichert, V. R.; Mathias, L. J. *Macromolecules* **1994**, *27*, 7030–7034.
(8) Lee, M. W.; Farha, O. K.; Hawthorne, M. F.; Hansch, C. H. *Angew. Chem., Int. Ed.* **2007**, *46*, 3018–3022.
(9) Farha, O. K.; Julius, R. L.; Lee, M. W.; Huertas, R. E.; Knobler, C. B.; Hawthorne, M. F. *J. Am. Chem. Soc.* **2005**, *127*, 18243–18251.
(10) Sanchez, C.; de A.A. Soler-Illia, G. J.; Ribot, F.; Lalot, T.; Mayer, C. R.; Cabuil, V. *Chem. Mater.* **2001**, *13*, 3061–3083.
(11) Blunt, M. O.; Russell, J. C.; Giménez-López, M. D. C.; Garrahan, J. P.; Lin, X.; Schröder, M.; Champness, N. R.; Beton, P. H. *Science* **2008**, *322*, 1077–1081.
(12) Mecozzi, S.; Rebek, J., Jr. *Chem. Eur. J.* **1998**, *4*, 1016–1022.
(13) Côté, A. P.; Benin, A. I.; Ockwig, N. W.; O'Keeffe, M.; Matzger, A. J.; Yaghi, O. M. *Science* **2005**, *310*, 1166–1170. El-Kaderi, H. M.; Hunt, J. R.; Mendoza-Cortés, J. L.; Côté, A. P.; Taylor, R. E.; O'Keeffe, M.; Yaghi, O. M. *Science* **2007**, *316*, 268–272.
(14) Tozawa, T.; Jones, J. T. A.; Swamy, S. I.; Jiang, S.; Adams, D. J.; Shakespeare, S.; Clowes, R.; Bradshaw, D.; Hasell, T.; Chong, S. Y.; Tang, C.; Thompson, S.; Parker, J.; Trewin, A.; Bacsa, J.; Slawin, A. M. Z.; Steiner, A.; Cooper, A. I. *Nat. Mater.* **2009**, *8*, 973–978.
(15) Maly, K. E. *J. Mater. Chem.* **2009**, *19*, 1781–1787.

We describe here the synthesis and detailed characterization of the homologous *p*-iodophenyl SQs $[p\text{-I-}C_6H_4SiO_{1.5}]_n$ ($n = 8$, 10, 12), along with their potential for symmetric functionalization, allowing the creation of diverse 3-D NBs and their thermal conversion to high-surface-area, microporous materials. The first step in this process was to develop a new synthetic route to pentagonal prismatic $[C_6H_5SiO_{1.5}]_{10}$. The $[p\text{-I-}C_6H_4SiO_{1.5}]_{8/10/12}$ series possesses equivalent chemical functionality but different symmetries and degrees of functionality, crucial for the investigation of structure−property relationships in subsequently synthesized derivatives and materials.

As part of our efforts to use these compounds as NBs, we recently described the synthesis of octaalkyne derivatives.[22,23] In future papers we will discuss the transformation of the octadiphenylethyne SQ into the octa-hexaphenylbenzene SQ and related compounds and thereafter into octagraphenes.[21] We will also report on the catalytic self-coupling of octa-trimethylsilylethynylphenyl SQ into microporous 3-D structures with specific surface areas (SSAs) >1000 m^2/g.[23]

In this paper, we report initial studies targeting microporous materials simply by decomposing these iodo compounds. Thus, each of the three iodophenyl SQs lose theoretical amounts of I_2 at ∼400 °C/N_2 in forming microporous cage structures with very high thermal stabilities, monomodal pore size distributions at the lower detection limit of 8 Å, and SSAs of ∼500−700 m^2/g.

Experimental Section

Materials. OPS and DPS were prepared using literature methods[24] or was a gift from Mayaterials, Inc., Ann Arbor, MI. ICl (1.0 M in dichloromethane) and other synthetic reagents were purchased from Sigma Aldrich and used as received. Dichloromethane was purchased from Burdick-Jackson or Sigma Aldrich. Solvents were dried over 4 Å molecular sieves.

Analytical Methods. Gel Permeation Chromatography (GPC). All GPC analyses were conducted on a Waters 440 system equipped with Waters Styragel columns (7.8 × 300, HT 0.5, 2, 3, 4) with RI detection using an Optilab DSP interferometric refractometer and THF as solvent. The system was calibrated using polystyrene standards and toluene as a reference.

Nuclear Magnetic Resonance (NMR). All ^{1}H NMR spectra were collected from samples dissolved in $CDCl_3$ and recorded on a Varian INOVA 400 MHz spectrometer. ^{1}H spectra were collected at 400 MHz using a 6000 Hz spectral width, a relaxation delay of 0.5 s, 30k data points, a pulse width of 38°, and $CHCl_3$ (7.24 ppm) as the internal reference. ^{13}C spectra were collected at 100 MHz using 25 141.4 Hz spectral width, a relaxation delay of 1.5 s, 75k data points, 40° pulse width with 256 repetitions, and $CHCl_3$ (77.23 ppm) as the internal reference.

Thermogravimetric Analyses (TGA/DTA). All TGA/DTA analyses were run on a 2960 simultaneous DTA-TGA Instrument (TA Instruments, Inc. New Castle, DE). Samples (15−25 mg) were loaded in alumina pans and ramped at 10 °C/min to 1000 °C in dry air at 60 mL/min.

Matrix-Assisted Laser Desorption/Time-of-Flight Spectrometry (MALDI-TOF). These measurements were carried out on a Micromass TofSpec-2E equipped with a 337 nm nitrogen laser in positive-ion reflectron mode using poly(ethylene glycol) as a calibration standard, dithranol as the matrix, and $AgNO_3$ as the ion source. Samples were prepared by mixing solutions of 5 parts matrix (10 mg/mL in THF), 5 parts sample (1 mg/mL in THF), and optionally 1 part $AgNO_3$ (2.5 mg/mL in water) and blotting the mixture on the target plate.

The resulting chromatograms were averaged and smoothed once using the Savitzky−Golay algorithm. The baseline was subtracted using a 99th order polynomial, and the spectra were centered using a channel width of half the full width at half-maximum.

FTIR Analyses for Thermolyzed Products. Infrared absorption spectra were collected on a Nicolet AVATAR 360 FTIR instrument. Samples were ground with KBr to make 1 wt % mixtures and pelletized. Nitrogen was purged for 10 min before data collection. Scans (32) were collected for each sample at a resolution of 4 cm^{-1}.

Surface Area. Nitrogen sorption isotherms were measured volumetrically at 77 K in the range $1.00 \times 10^{-3} \leq P/P_0 \leq 1.00$ with a NOVA 4200e instrument by Quantachrome Instruments (Boynton Beach, FL), running version 2.1 of the NovaWin2 software package. Ultrahigh-purity N_2 (99.999%) from Cryogenic Gases was used as received.

Pore Size Distribution. Argon sorption experiments were performed at 87 K in the range $1.00 \times 10^{-3} \leq P/P_0 \leq 1.00$ with an Autosorb-1C by Quantachrome Instruments. Ultrahigh-purity Ar (99.999%) was purchased from Cryogenic Gases and used as received. Pore size distributions were calculated using the Nonlinear Density Functional Theory (NLDFT) kernel as implemented in version 1.2 of the ASWin software package.

XRD Studies. Heat-treated samples were characterized using a Rigaku rotating anode goniometer. Powder samples were prepared by placing ∼100 mg of powder on amorphous silica slides for data collection. Cu Kα radiation ($\lambda = 1.54$ Å) with a Ni filter was used with a working voltage and current of 40 kV and 100 mA, respectively. Scans were continuous from 20−80° 2θ with a continuous scan speed of 1.5° 2θ/min, sampled at 0.02° 2θ. Jade software (Materials Data Inc., Version 7.0) was used to compare peak positions and relative intensities to PDF files of standard materials. Jade 7.0 was also used to determine the materials' phase compositions by simulation.

Scanning Electron Microscopy (SEM). A field emission SEM instrument (FEI Nova Nanolab with EDAX attachment) was used to examine thermolyzed material morphologies (operating voltage 10.0−20.0 kV). Samples were dispersed in EtOH, and a drop of the dispersed powder was placed on an aluminum SEM stub and allowed to dry in air for 1 h on a hot plate. Powders were sputter-coated with 1−4 nm of Au−Pd to reduce charging effects.

Synthetic Methods. Synthesis of Octaiodophenylsilsesquioxane. This was carried out using our recently published route.[25]

Dodecaiodophenylsilsesquioxane I_{12}DPS. In an oven-dried, single-neck 500 mL flask under flowing N_2 was added 250 mL of 1.0 M ICl/CH_2Cl_2 solution. The solution was cooled to −60 °C using a dry ice/ethylene glycol/ethanol bath,[26] and 20.5 g (25.8 mmol) of powdered DPS was added at an approximate rate of 5 g/min with stirring. HCl evolution began within 1 min of DPS addition. Flowing N_2 (5−10 mL/min) flushes the HCl from the reaction system. Residual DPS sticking to the sides of the flask was washed into the reaction solution with 40 mL of CH_2Cl_2. The

(16) Neel, N.; Kroger, J.; Limot, L.; Berndt, R. *Nano Lett.* **2008**, *8*, 1291–1295.
(17) Lutich, A. A.; Jiang, G.; Susha, A. S.; Rogach, A. L.; Stefani, F. D.; Feldmann, J. *Nano Lett.* **2009**, *9*, 2636–2640.
(18) Giacalone, F.; Segura, J. L.; Martîn, N.; Guldi, D. M. *J. Am. Chem. Soc.* **2004**, *126*, 5340–5341.
(19) Zhi, L.; Müllen, K. *J. Mater. Chem.* **2008**, *18*, 1472–1484.
(20) Hill, J. P.; Jin, W.; Kosaka, A.; Fukushima, T.; Ichihara, H.; Shimomura, T.; Ito, K.; Hashizume, T.; Ishii, N.; Aida, T. *Science* **2004**, *304*, 1481–1483.
(21) Roll, M. F.; Kampf, J. W.; Laine, R. M. Manuscript in preparation.
(22) Asuncion, M. Z.; Roll, M. F.; Laine, R. M. *Macromolecules* **2008**, *41*, 8047–8052.
(23) Kim, Y.; Koh, K.; Roll, M. F.; Laine, R. M.; Matzger, A. J. Submitted for publication in *Macromolecules*.
(24) Kim, S.-G.; Sulaiman, S.; Fargier, D.; Laine, R. M. In *Materials Syntheses: A Practical Guide*; Schubert, U., Hüsing, N., Laine, R., Eds.; Springer-Verlag: Weinheim, Germany, 2008; pp 179−182.
(25) Roll, M. F.; Asuncion, M. Z.; Kampf, J.; Laine, R. M. *ACS Nano* **2008**, *2*, 320–326.
(26) Lee, D. W.; Jensen, C. M. *J. Chem. Educ.* **2000**, *77*, 629.

reaction mixture was stirred for 24 h at temperature, warmed to room temperature with stirring over another 24 h, and quenched with 300 mL of ~1 M sodium metabisulfite.

When all the ICl was consumed and quenched, the organic layer was extracted and washed 3× with water, filtered, and dried over anhydrous sodium sulfate. The volume was subsequently reduced by rotary evaporation, generating a white oil, which was placed in a freezer overnight. Thereafter, the cold solid was treated with 250 mL of ethyl acetate, which dissolved the noncrystalline material, allowing recovery of the crystalline material by filtration. This material was washed with an additional 100 mL of ethyl acetate.

The microcrystalline material was recrystallized from *m*-xylene with ~1% dodecane (to assist crystallization). The large crystals that were isolated were redissolved in 150 mL of hot tetrahydrofuran and precipitated into 750 mL of cold methanol. The precipitate was filtered, washed with methanol, and dried under vacuum to yield 5.6 g of white powder (14% of theoretical yield for complete conversion). The noncrystalline material was collected and precipitated into 1 L of cold methanol, yielding 29 g of white powder. Total yield: 34.6 g, 86% of theory.

Decaphenylsilsesquioxane. In an oven-dried 200 mL round-bottom flask with a magnetic stir bar is added 3 g (1.93 mmol) of dodecaphenylsilsesquioxane followed by 260 mg (0.984 mmol) of 18-crown-6 and 160 mg (1.04 mmol) of BaO. A 100 mL portion of *m*-xylene was added to the flask, which was placed in a heating mantle on a magnetic stir plate. After stirring commenced, a condenser was added and a nitrogen inlet was attached. A variac controlled heating mantle was used to bring the solution to reflux. After 1 day, the heating mantle was removed and stirring halted. The solution was allowed to settle and cool for ~1 h. At this time ~1 mL of concentrated aqueous HCl was added and stirring was restarted. After 30 min, the mixture was again allowed to settle and the organic layer was decanted from insoluble precipitates and water. A 10 mL portion of toluene was added to the flask, and the organic layer was again decanted. The combined organic layer was filtered and the solvent removed by distillation until only a few milliliters of yellow solution remained. The flask was again cooled, and a white precipitate formed. A 100 mL portion of tetrahydrofuran was added, and the resulting suspension was stirred overnight. The suspension was filtered, and the tetrahydrofuran was removed by rotary evaporation, yielding a solid which was triturated in a minimum volume of warm cyclohexane and filtered. The white, crystalline solid was washed with 1 mL of cyclohexane and dried, giving 500 mg (0.387 mmol) of decaphenylsilsesquioxane. Single crystals suitable for X-ray diffraction could be grown by the slow evaporation of CH_2Cl_2/toluene solutions.

Decaiodophenylsilsesquioxane I_{10}dPS. In an oven-dried, single-neck 50 mL Schlenk flask under flowing N_2 was added 13 mL of 1.0 M ICl/CH_2Cl_2 solution. The solution is cooled to −60 °C using a dry ice/ethylene glycol/ethanol bath,[26] and 1.1 g (0.63 mmol) of recrystallized decaphenylsilsesquioxane (dPS) was added over ~1 min with stirring. HCl evolution began within 1 min of dPS addition. Flowing N_2 (5−10 mL/min) flushed the HCl from the reaction system. Residual dPS sticking to the sides of the flask was washed into the reaction solution with 2 mL of CH_2Cl_2. The reaction mixture was stirred for 24 h while being warmed to room temperature. At this time the reaction was quenched with 10 mL of ~1 M sodium metabisulfite.

When all the ICl in the organic layer was consumed and quenched, 100 mL of ethyl acetate and 50 mL of brine were added and the organic layer was extracted. The organic layer was subsequently washed once with saturated sodium bicarbonate and once with brine, extracted, and filtered. The clear organic layer was allowed to evaporate in the fume hood until roughly 50 mL of solvent remained. The colorless crystals that were generated (380 mg) were separated by decanting the supernatant, which was subsequently reduced to an oil by rotary evaporation. A minimum amount of tetrahydrofuran was added (~5 mL), and the clear solution was precipitated into 100 mL of methanol. The flask was placed in the freezer overnight, and after 24 h 1.37 g of white powder was recovered by filtration, for a combined yield of 1.75 g (80% of the theoretical amount).

Thermolysis Reactions. Thermolysis was conducted by heating samples of I_8OPS, I_{10}dPS, and I_{12}DPS under N_2 (~5 mL/min, across tube mouth) in a Lindberg 55035 mini-Mite tube furnace from RT to 300 °C at 5 °C/min and then 0.1 °C/min to 385 °C and held for ~4−6 h, giving the products denoted T-I_8OPS, T-I_{10}dPS, and T-I_{12}DPS. One sample of I_8OPS, denoted T-I_8OPS (rapid), was thermolyzed at a heating rate of 5 °C/min to 375 °C and then 0.1 °C/min to 385 °C and held for 24 h for comparison. Crystals of iodine were found to form in the reaction tube near the mouth of the furnace. At the end of the reaction time, the furnace and sample were cooled to ambient. The samples were then weighed, and BET, XRD, FTIR, and TGA analyses were conducted.

Results and Discussion

In general, cubic SQs, Q_8 $[RMe_2SiOSiO_{1.5}]_8$ and T_8 $[RC_6H_4SiO_{1.5}]_8$ or POSS compounds,[27−30] with a D4R-like silica core structure, are easily prepared in comparison to the cubane and prismane families of compounds.[1,4,5] These SQs have high thermal stabilities (>500 °C in air for octaphenyl SQ, OPS[31]) and a wide variety of possible functional groups.[29,30]

The exploration of pentagonal symmetry and quasi-crystals in small-molecule tiling patterns,[32−34] polymers,[35] polyoxometalates,[36] and metals[37,38] has been a topic of many recent reports. Fivefold symmetry is rare among reported macromolecules, though Bauert et al. recently discussed the 2-D ordering of fivefold symmetric polyaromatic hydrocarbons on surfaces.[35] Two T_{10} SQ crystal structures are found in the Cambridge Crystallographic Database, the decamethylsilsesquioxane[39] and the monophenyl-nonahydrido-decaSQ.[40] The decahydrido SQ crystal structure, based on solid-state X-ray diffraction, was reported by Bürgi et al.,[41] while structure based on the gas-phase electron diffraction was recently reported by Wann et al.[42]

Dodecafunctional SQs are also rare, with only the crystal structures of dodecahydrido SQ[43] and dodecaphenyl SQ (DPS)

(27) Laine, R. M. *J. Mater. Chem.* **2005**, *15*, 3725–3744.
(28) Baney, R. H.; Itoh, M.; Sakakibara, A.; Suzuki, T. *Chem. Rev.* **1995**, *95*, 1409–1430.
(29) Voronkov, M. G.; Lavrent'yev, V. I. *Top. Curr. Chem.* **1982**, *102*, 199–236.
(30) Cordes, D. B.; Lickiss, P. D.; Rataboul, F. *Chem. Rev.* **2010**, *110*, 2081–2173.
(31) Brown, J. F., Jr.; Vogt, L. H.; Prescott, P. I. *J. Am. Chem. Soc.* **1964**, *86*, 1120–1125.
(32) Bauert, T.; Merz, L.; Bandera, D.; Parschau, M.; Siegel, J. S.; Ernst, K.-H. *J. Am. Chem. Soc.* **2009**, *131*, 3460–3461.
(33) Zhou, Z.; Harris, K. D. M. *J. Phys. Chem. C* **2008**, *112*, 16186–16188.
(34) Guillermet, O.; Niemi, E.; Nagarajan, S.; Bouju, X.; Martrou, D.; Gourdon, A.; Gauthier, S. *Angew. Chem., Int. Ed.* **2009**, *48*, 1970–1973.
(35) Hayashida, K.; Dotera, T.; Takano, A.; Matsushita, Y. *Phys. Rev. Lett.* **2007**, *98*, 195502.
(36) Schäffer, C.; Merca, A.; Bögge, H.; Todea, A. M.; Kistler, M. L.; Liu, T.; Thouvenot, R.; Gouzerh, P.; Müller, A. *Angew. Chem., Int. Ed.* **2009**, *48*, 149–153.
(37) Shechtman, D.; Blech, I.; Gratias, D.; Cahn, J. W. *Phys. Rev. Lett.* **1984**, *53*, 1951–1953.
(38) Levin, D.; Steinhardt, P. J. *Phys. Rev. Lett.* **1984**, *53*, 2477–2480.
(39) Baidina, I. A.; Podberezskaya, N. V.; Borisov, S. V.; Alekseev, V. I.; Martynova, T. N.; Kabnev, A. N. *J. Struct. Chem.* **1980**, *21*, 352–355.
(40) Calzaferri, G.; Claudia Marcolli, C.; Imhof, R.; Tornroos, K. W. *J. Chem. Soc., Dalton Trans.* **1996**, *1996*, 3313–3322.
(41) Burgi, H.-B.; Tornroos, K. W.; Calzaferri, G.; Burgy, H. *Inorg. Chem.* **1993**, *32*, 4914–4919.
(42) Wann, D. A.; Rataboul, F.; Reilly, A. M.; Robertson, H. E.; Lickiss, P. D.; Rankin, D. W. H. *Dalton Trans.* **2009**, 6843–6848.
(43) Tornroos, K. W.; Burgi, H.-B.; Calzaferri, G.; Burgy, H. *Acta Crystallogr., Sect. B* **1995**, *51*, 155–161.

reported.[44,45] Surprisingly, both structures possess D_{2d} symmetry rather than hexagonal-prismatic (D6R) symmetry.[43–45] Agaskar et al. described the synthesis of dodeca(trimethylsiloxy) SQ but did not report a single-crystal structure.[46] A recent report by Takahashi et al. describes the synthesis of a dodecaamino DPS system, its use in forming epoxy resin nanocomposites, and their mechanical properties.[47]

In the following sections, we briefly describe general syntheses of the starting SQs, focusing primarily on the synthesis and isolation of the decamer and thereafter the synthesis of the iodo derivatives.

Synthesis and Physical Characterization of Decaphenylsilsesquioxane. Phenyltrichlorosilane ($PhSiCl_3$) can be hydrolyzed and condensed to form polyphenylsilsesquioxane $[PhSiO_{1.5}]_n$ (PPS), as described by Brown[31] and others.[24,48,49] OPS can be synthesized from PPS by reacting it with a catalytic amount of KOH in toluene under water-starved conditions. However, as described elsewhere, in our hands it has proved best to first convert $PhSiCl_3$ to a polymeric ethoxy derivative and then react this intermediate in toluene with catalytic amounts of KOH under water-starved conditions at reflux such that the resulting homogeneous solution continuously precipitates OPS.[24] The crystalline, insoluble product may be isolated by filtration of the reaction solution at the end of the desired reaction period.[24,31,48,49]

In contrast, dPS has only been isolated, without a reported yield, by Brown et al. as the most soluble crystalline product of KOH-equilibrated PPS in toluene or benzene by fractional recrystallization of the soluble products.[31] In contrast to OPS, where isolation is accomplished by precipitation of the desired product, the high solubility of dPS hinders its separation from PPS, which is also very soluble. Since the reaction solution during base-catalyzed equilibration is populated by a large number of open- and closed-cage polyhedral species, the isolation of a single soluble cage species from the equilibrium is difficult at best.[31,48]

Because OPS and DPS have been well characterized,[24,31,48,49] the following discussion centers on the synthesis and characterization of dPS. Although KOH is often used to catalyze SQ rearrangements, alkali-metal picrates form complexes with SQ cages.[50] To separate the possible effects of complexation (and solubilization) from rearrangement processes, it was desirable to use a catalyst anticipated to have minimal interactions with the cage.

Previous work showed that $Ba(OH)_2$ does not react with OPS derivatives in toluene or xylenes, even under reflux.[51] However, the combination of $Ba(OH)_2$ and *catalytic* 18-crown-6 gives an active catalyst for rearrangement. If BaO is substituted for $Ba(OH)_2$, any adventitious water is removed by the desiccating action of BaO.[52]

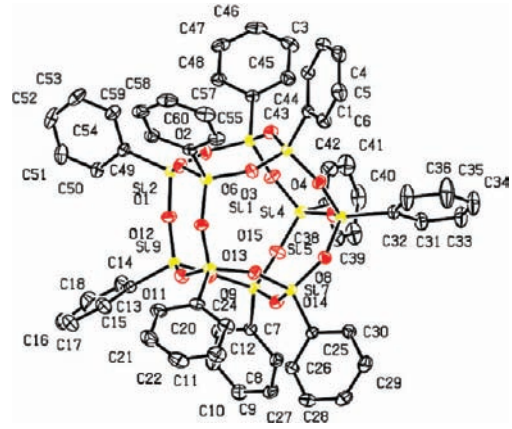

Figure 1. Thermal ellipsoid plot (at the 50% probability level) of decaphenylsilsesquioxane−toluene. Hydrogen atoms and the toluene solvate are omitted for clarity. Full data are provided in the Supporting Information.

Table 1. Crystal Structure Data for Decaphenylsilsesquioxane−Toluene (dPS·(Toluene))

empirical formula	$C_{60}H_{50}Si_{10}O_{15}\cdot C_7H_8$
space group	$P\bar{1}$, triclinic
unit cell dimens	
a, Å	12.5377(9)
b, Å	24.6836(17)
c, Å	35.061(2)
α, deg	72.706(1)
β, deg	80.434(1)
γ, deg	87.395(1)
unit cell vol, Å^3	10 157.8(12)
Z; density, Mg/m^3	6; 1.358
R factor ($I > 2\sigma(I)$), %	4.1

Combining these insights, we find that anhydrous, base-catalyzed rearrangement of $[PhSiO_{1.5}]_{12}$ under high dilution (3 g of DPS/100 mL of *m*-xylene) allows isolation of dPS. Specifically, $[PhSiO_{1.5}]_{12}$ is equilibrated using catalytic BaO/18-crown-6 in *m*-xylene at reflux for 1 day (see the Experimental Section). dPS is isolated in ∼15% yield by repeated recrystallization from toluene.

Since the ^1H and ^{13}C NMR spectra have not been reported, they are included as Figures S1 and S2 with assignments. The MALDI-TOF spectrum of the dPS is given in Figure S3 (Figures S1−S3 are given in the Supporting Information). Single crystals suitable for X-ray analysis were grown from toluene. The dPS crystal structure is shown in Figure 1 without the toluene solvate molecules. Crystallographic data are presented in Table 1.

DodecaphenylSQ (DPS) was first isolated by Brown et al. in ∼60% yield by equilibrating PPS with catalytic KOH in refluxing THF at 0.9 M $[PhSiO_{1.5}]_n$.[31] The insoluble product, isolated as a 1:2 DPS−THF clathrate, is much less soluble than OPS in THF.[31] OPS and DPS are available in commercial quantities and offer the multifunctionality and 3-D symmetry necessary for nano building blocks. dPS, while not commercially available, will be useful for comparing physical properties and chemical reactivities.

We now discuss the iodination of the OPS, dPS, and DPS systems as a route to symmetrically functionalized nano building blocks with three quite different geometries.

Iodination of Polyhedral Phenyl SQs. Previous studies have shown that the inorganic $(-SiO_{1.5})_n$ ($n = 8, 12$) core and the linking C−Si bonds are remarkably stable to strong electrophiles and acids, allowing a wide variety of electrophilic reactions to

(44) Clegg, W.; Sheldrick, G. M.; Vater, N. *Acta Crystallogr., Sect. B* **1980**, *36*, 3162–3164.
(45) Shklover, V. E.; Ovchinnikov, Y. E.; Struchkov, Y. E.; Levitskii, M. M.; Zhdanov, A. A. *Organomet. Chem. USSR* **1988**, *1*, 696–698.
(46) Agaskar, P. A.; Day, V. W.; Klemerer, W. G. *J. Am. Chem. Soc.* **1987**, *109*, 5554–5556.
(47) Takahashi, K.; Sulaiman, S.; Katzenstein, J. M.; Snoblen, S.; Laine, R. M. *Aust. J. Chem.* **2006**, *59*, 564–570.
(48) Pakgamsai, C.; Kobayashi, N.; Koyano, M.; Sasaki, S.; Kawakami, Y. *J. Polym. Sci., Part A: Polym. Chem.* **2004**, *42*, 4587–4597.
(49) Olsson, K.; Gronwall, C. *Ark. Kemi* **1961**, *17*, 529–540.
(50) Dittmar, U.; Marsmann, H. C.; Rikowski, E. *Organosilicon Chem. III (Muench. Silicontage), 3rd* **1998**, 395–399.
(51) James, N. D.; Roll, M. F. Unpublished results.
(52) Booth, H. S.; McIntyre, L. H. *Ind. Eng. Chem.* **1930**, *2*, 12–15.

Scheme 1. Functionalization of I_8OPS via Standard Coupling Chemistries[a,25]

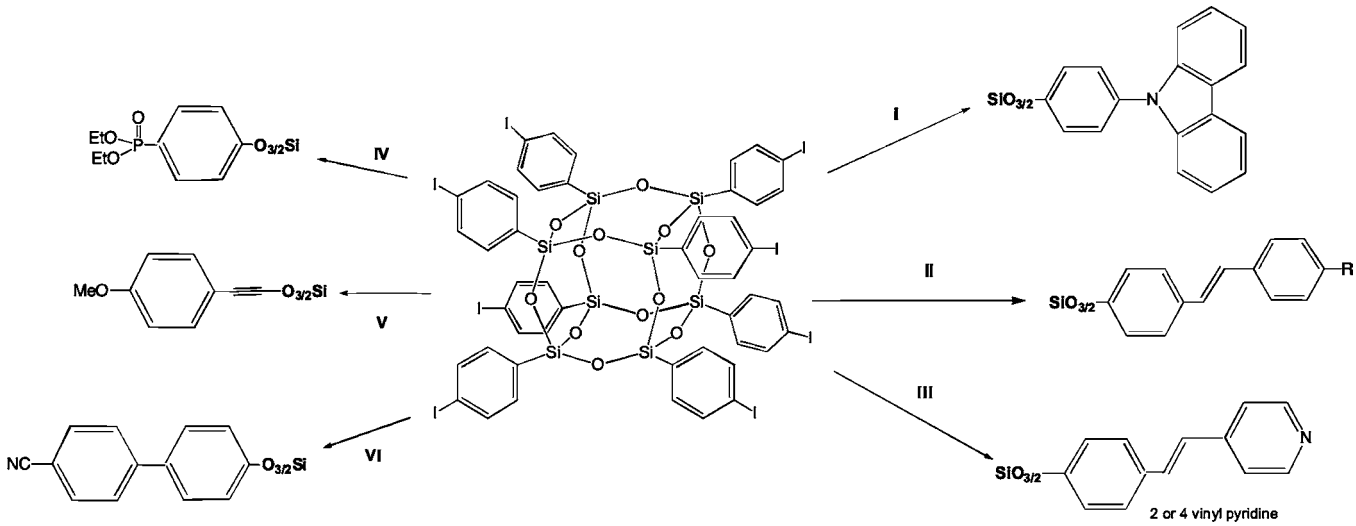

[a] Legend: (I) Cu^+/carbazole; (II) Heck reaction, Pd/R-styrene/amine; (III) Heck reaction, Pd/vinyl-2/4-pyridine/amine; (IV) Ni^0/triethyl phosphite; (V) Sonogashira reaction, Pd/alkyne/amine; (VI) Suzuki reaction, Pd/boronic acid/phase transfer agent.

be effected on all of the phenyl systems.[25,47,49,53] In general, halogenation requires a Lewis acid catalyst to polarize a diatomic halogen, X_2[52–54] generating an electrophilic halogen "X^+", that can react with aromatic rings.[54,55] In iodination, an oxidizing agent is normally needed to generate I^+ in situ.[54–56]

Vogel suggests using fuming nitric acid as the oxidant in the iodination of benzene.[56] Alternately, the hypervalent iodine reagent bis(trifluoroacetoxy)iodobenzene (BFIB) can be used: e.g., as the oxidant in the synthesis of tetrakis(*p*-iodophenyl)-adamantane[57] and hexakis(*p*-iodophenyl)benzene.[58] In contrast, the less expensive iodine monochloride (ICl) is permanently polarized and can act as an effective, stable I^+ source.[25] ICl is commercially available in methylene chloride solution, the best solvent for OPS, which reduces the heterogeneity of the reaction.

Iodinated aromatics, including the previously reported I_8OPS, tetrakis(*p*-iodophenyl)adamantane,[6,7,57] and hexakis(*p*-iodophenyl)benzene,[58] are useful precursors for the synthesis of complex molecular systems, such as our targeted nano building blocks. One reason is that the extensive catalytic C−C and C−heteroatom cross-coupling reactions developed over the past few decades allows multiple types of functionalities to be incorporated.[59−67] Examples include the Heck,[59,60] Stille,[59] Suzuki,[59,61] and Sonogashira[59,62] reactions. Catalytic cross-coupling also allows incorporation of heteroatoms via amination,[63,64] phosphonation,[65] etherfication,[66] or thioetherification.[67] We have previously described examples of such reactions for I_8OPS, as shown in Scheme 1.[25]

Scheme 2. Iodination of Polyhedral Phenylsilsesquioxanes

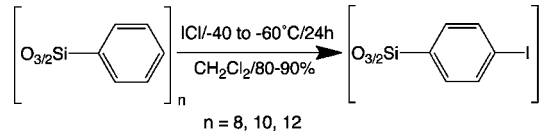

Table 2. Characterization of the Homologous Iodophenyl SQ

compd	yield (%)	crystalline yield (%)	CY[a] calcd	CY[a] found	MALDI (Da) calcd	MALDI (Da) found
I_8OPS	90	30−40%	23.5	22	2148.6 (Ag^+)	2148
I_{10}dPS	80	30−40%	23.5	23	2658.72	2657
I_{12}DPS	90	20%	23.5	24	3168.9	3167.3

[a] CY = ceramic yield in air/10 °C/min.

As described previously,[25] for operational simplicity, initial reactions of OPS with ICl in methylene chloride (see Scheme 2) were run at ambient temperature, but we were pleasantly surprised to discover that iodination of OPS with ICl at −40 °C and precipitation of the crude I_8OPS in methanol gave a 90% yield. Recrystallization from ethyl acetate provided 30−40% colorless crystals of I_7OPS and I_8OPS on filtration, on the basis of octasubstitution.

Though initial NMR data suggested para substitution, oxidative cleavage with F^- was used to produce the iodophenols, allowing the substitution patterns of the crystalline and non-crystalline fractions to be quantified.[25,53] Recrystallization gives 30−40% of the theoretical yield by mass and removes the I_9 isomer. GC/MS analysis of the resulting iodophenols shows *p*-iodophenol and only traces of phenol or other iodophenols.[25]

Fortunately, iodination of dPS and DPS is also facile using ICl at −40 °C. In fact, as suggested in Table 2, all of the compounds have exactly the same stoichiometry. For the decamer, its high solubility hinders isolation because of the small

(53) Brick, C. M.; Tamaki, R.; Kim, S.-G.; Asuncion, M. Z.; Roll, M.; Nemoto, T.; Ouchi, Y.; Chujo, Y.; Laine, R. M. *Macromolecules* **2005**, *38*, 4655–4660.
(54) Morrison, R. T.; Boyd, R. N. *Organic Chemistry*, 2nd ed.; Allyn and Bacon, Inc.: Boston, 1966.
(55) Galli, C. *J. Org. Chem.* **1991**, *56*, 3238–3245.
(56) Vogel, A. *Practical Organic Chemistry*; Wiley: New York, 1966.
(57) Reichert, V. R.; Mathias, L. J. *Macromolecules* **1994**, *27*, 7024–7029.
(58) Kobayashi, K.; Kobayashi, N.; Ikuta, M.; Therrien, B.; Sakamoto, S.; Yamaguchi, K. *J. Org. Chem.* **2005**, *70*, 749–752.
(59) Babudri, F.; Farinola, G. M.; Naso, F. *J. Mater. Chem.* **2004**, *14*, 11–34.
(60) Nicolaou, K. C.; Bulger, P. G.; Sarlah, D. *Angew. Chem., Int. Ed.* **2005**, *44*, 4442–4489.
(61) Miyaura, N.; Suzuki, A. *Chem. Rev.* **1995**, *95*, 2457–2483.
(62) Negishi, E.; Anastasia, L. *Chem. Rev.* **2003**, *103*, 1979–2017.
(63) Hartwig, J. F.; Kawatsura, M.; Hauck, S. I.; Shaughnessy, K. H.; Alcazar-Roman, L. M. *J. Org. Chem.* **1999**, *64*, 5575–5580.
(64) Wolfe, J. P.; Buchwald, S. L. *J. Org. Chem.* **1997**, *62*, 6066–6068.
(65) Balthazor, T. M.; Grabiak, R. C. *J. Org. Chem.* **1980**, *45*, 5425–5426.
(66) Vorogushin, A. V.; Huang, X.; Buchwald, S. L. *J. Am. Chem. Soc.* **2005**, *127*, 8146–8149.
(67) Fernandez-Rodriguez, M. A.; Hartwig, J. F. *J. Org. Chem.* **2009**, *74*, 1663–1672.

Table 3. NMR Characterization of the Homologous $[p\text{-I-}C_6H_4SiO_{1.5}]_{8/10/12}$

compd	^{1}H NMR (ppm)	^{13}C NMR (ppm)
I_8OPS	7.73−7.71, 7.37−7.35	137.38, 135.20, 128.07, 99.66
I_{10}dPS	7.64−7.62, 7.20−7.18	137.43, 135.53, 128.91, 98.94
I_{12}DPS	7.63−7.61, 7.53−7.51, 7.18−7.16, 7.05−7.02	137.40, 137.26, 135.4, 135.3, 129.04, 98.97

solubility differences between the symmetrically and unsymmetrically substituted isomers. Analogous to the high solubility of the decamer in toluene/methanol solutions, precipitation of I_{10}dPS in methanol leads to somewhat lower yields, 80%. Recrystallization from ethyl acetate provided 30−40% of the theoretical yields as colorless crystals of decakis(*p*-iodophenyl) SQ. Single crystals suitable for X-ray diffraction studies were grown by slow cooling of hot, saturated ethyl acetate solutions.

For the DPS, the I_{12}DPS product is recovered in 90% yield and the perfectly symmetrically substituted material is recovered after recrystallization from *m*-xylene in 20% yield. Since the probability of synthesizing a crystalline, symmetrically substituted molecule is the product of the probabilities of each independent substitution, this is reasonably lower than the yield of the crystalline octamer. The remaining ∼70% of the reaction product is isolated after precipitation into methanol as white powder, shown by MALDI-TOF to be a mixture of the para I_{10}−I_{13} species.

NMR spectroscopy is valuable in characterization of the $[p\text{-I-}C_6H_4SiO_{1.5}]_{8/10/12}$ compounds. The T_8 and T_{12} compounds offer relatively simple ^{1}H NMR spectra (see the Supporting Information), with two multiplet resonances consistent with para substitution. One notable feature is the slight (ca. 0.15 ppm) upfield shift seen in the ^{1}H spectrum of the decamer. This indicates slight differences in the electronic nature of the T_8 and T_{10} cages (Table 3).

As discussed by Rikowski and Marsmann,[68] each vertex silicon in the octamer belongs to three 8-membered rings. However, in the decamer, each vertex silicon belongs to two 8-membered rings and one 10-membered ring. In the dodecamer, the situation is more complex.

Figure 2 provides the DPS single-crystal structure[44] from the Cambridge Crystallographic Database, revealing the presence of eight "equatorial" phenyl groups in violet, where each vertex silicon belongs to one 8-membered ring and two 10-membered rings. There are four "polar" phenyl groups in blue, where each vertex silicon belongs to two 8-membered rings and one 10-membered ring. Rikowski and Marsmann[68] find that the higher strain of the 4-membered ring is manifested as an *upfield* shift in a ^{29}Si spectrum of ∼2 ppm from ∼65 ppm between the octamer and decamer, depending on the organic group.

This same effect is found in the ^{1}H NMR spectra of $[p\text{-I-}C_6H_4SiO_{1.5}]_{8/10/12}$. Table 3 (Figures S4 and S5, Supporting Information) shows that each multiplet is shifted ca. 0.1−0.2 ppm upfield in each vertex which is part of a 5-membered ring. The ^{1}H NMR spectrum of $[p\text{-I-}C_6H_4SiO_{1.5}]_{12}$ shows two pairs of multiplets with a 1:2 integration corresponding to the symmetrically substituted polar and equatorial phenyls (Figure S6, Supporting Information). The small additional peaks in the spectrum likely belong to traces of *meta* or *ortho* iodinated phenyls, ∼4% by integration.

Octa- and deca-(*p*-iodophenyl)SQ are also characterized by relatively simple ^{13}C NMR spectra (Figures S7 and S8,

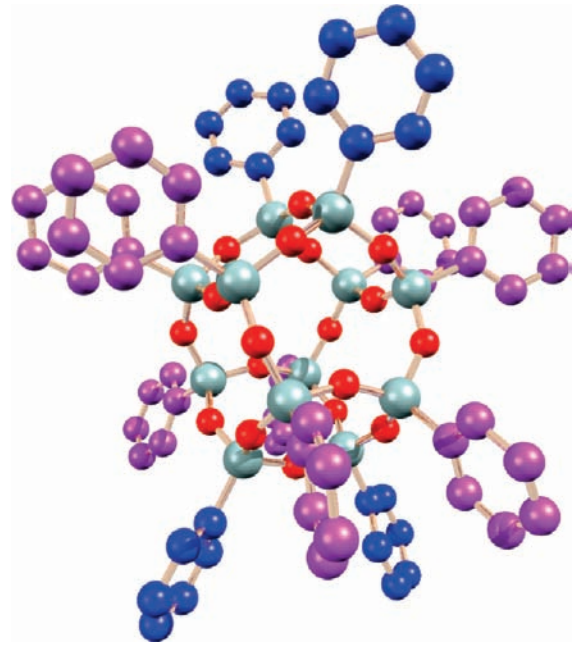

Figure 2. Different chemical environments in DPS. "Equatorial" phenyls are shown in purple and "polar" phenyls in blue.[39]

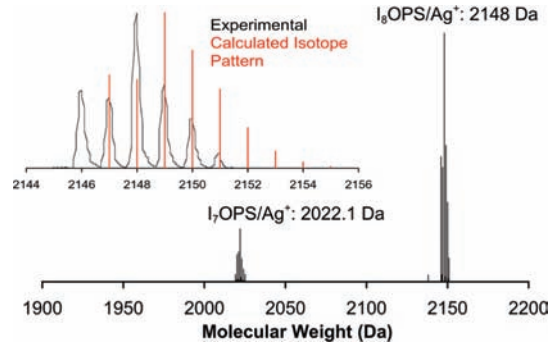

Figure 3. MALDI-TOF spectrum of recrystallized I_8OPS (dithranol/$AgNO_3$).

Supporting Information). Proton-decoupled (see the Experimental Section) spectra indicate that peaks in the decamer are shifted upfield 0.3−1 ppm relative to those in the octamer (Table 3). The proton-decoupled ^{13}C spectrum of the dodecamer in Figure S9 (Supporting Information) shows two distinct pairs of resonances, as expected from the ^{1}H NMR spectrum.

MALDI-TOF analysis indicates that these compounds have relatively narrow mass distributions (Figures 3−5). The breadth of the distribution increases from two peaks for the octamer to three peaks for the decamer and dodecamer. The relatively higher insolubility and larger size of the dodecamer may lead it to crystallize more rapidly from *m*-xylene, incorporating molecules with some unsubstituted phenyls.

In each case the calculated isotope distribution is higher than the experimental result. Since MALDI-TOF is a "time of flight" experiment, one possible factor in this could be the differences in desorption times between the SQ molecule and the polymer PEG calibrant. One could expect that a polymer chain has a larger degree of interaction and possibly entanglement with neighboring molecules and surfaces. The SQ compounds, on the other hand, are compact and rigid and might be expected to desorb more rapidly, thus reducing their "time of flight" and their apparent mass relative to the calibration polymer.

(68) Rikowski, E.; Marsmann, H. C. *Polyhedron* **1997**, *16*, 3357–3361.

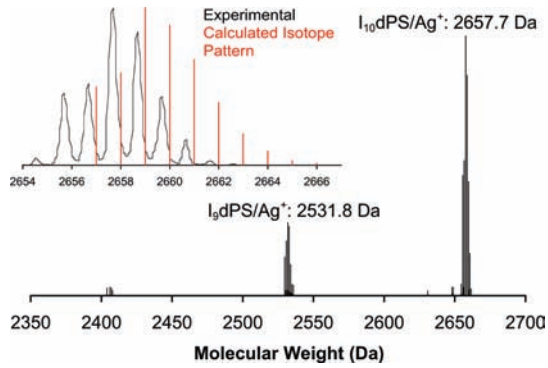

Figure 4. MALDI-TOF spectrum of I_{10}dPS (dithranol/$AgNO_3$).

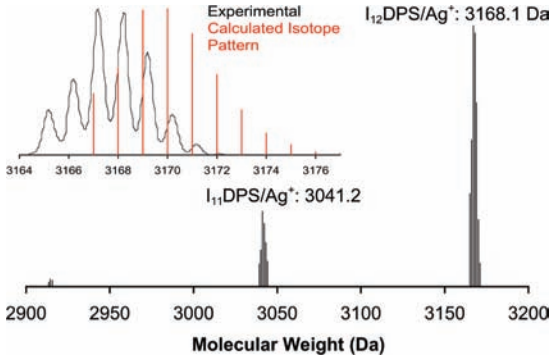

Figure 5. MALDI-TOF spectrum of I_{12}DPS (dithranol/$AgNO_3$).

Figure 6 provides FTIR spectra showing nearly perfect overlap, as might be expected. The ν(Si−O−Si) bands of the core are seen from 1200 to 1000 cm^{-1} with a maximum at 1130 cm^{-1}. The contributions from the aromatic rings are seen at 3100−3000 (ν C−H), 1575−1500 (ν/δ C═C), and 800−750 (δ(C−H)) cm^{-1}.

Crystal Structure Analyses of $[p\text{-I-}C_6H_4SiO_{1.5}]_{8/10/12}$. The pertinent data for the refined crystal structures of the homologous iodophenylsilsesquioxanes are presented in Table 4. X-ray-quality crystals of I_8OPS were grown from hot ethyl acetate. Single-crystal X-ray diffraction analysis reveals that I_8OPS crystallizes in the tetragonal space group *I*4/*m*. The unit cell contains four molecules with a total volume of 8618.9 $Å^3$. The SQUEEZE subroutine of the PLATON[69] suite was used to account for the scattering from a disordered ethyl acetate solvent molecule. This algorithm determines areas of possible solvent inclusion, calculates their effect on the structure factor, and incorporates the effect into the refinement.[69b] Figure 7 shows the final refinement of the structure.

Table 4. Crystal Structure Data for $[p\text{-I-}C_6H_4SiO_{1.5}]_{8/10/12}$

	$[p\text{-I-}C_6H_4SiO_{1.5}]_8$[25]	$[p\text{-I-}C_6H_4SiO_{1.5}]_{10}$	$[p\text{-I-}C_6H_4SiO_{1.5}]_{12}$
space group	*I*4/*m*, tetragonal	*C*2/*c*, monoclinic	*C*2/*c*, monoclinic
unit cell dimens			
a, Å	20.0403(11)	28.054(2)	32.082(9)
b, Å	20.0403(11)	15.6168(11)	14.704(4)
c. Å	21.4606(12)	22.3246(16)	28.755(8)
α, deg	90	90	90
β, deg	90	108.859(1)	118.438(4)
γ, deg	90	90	90
unit cell vol, $Å^3$	8618.9	9255.7	11 927.9
Z; density, Mg/m^3	4; 1.641	4; 1.831	4; 1.941
R factor ($I > 2\sigma(I)$), %	7.4 (9.7)[a]	4.6 (6.6)[a]	9.2

[a] Before use of SQUEEZE[69] (see the Experimental Section) to account for disordered solvent.

X-ray-quality crystals of I_{10}OPS were grown from hot ethyl acetate. Single-crystal X-ray diffraction analysis revealed that I_{10}OPS crystallizes in the monoclinic space group *C*2/*c*, as does the T_{12} compound. The unit cell contains four molecules with a total volume of 9255.7 $Å^3$. The SQUEEZE subroutine of the PLATON suite was used to account for the scattering from disordered ethyl acetate solvent molecules. Figure 8 shows the final refinement of the structure.

X-ray-quality crystals of I_{12}DPS were grown from hot *m*-xylene with 5% tetradecane. Single-crystal X-ray diffraction analysis shows that I_{12}DPS crystallizes in the monoclinic space

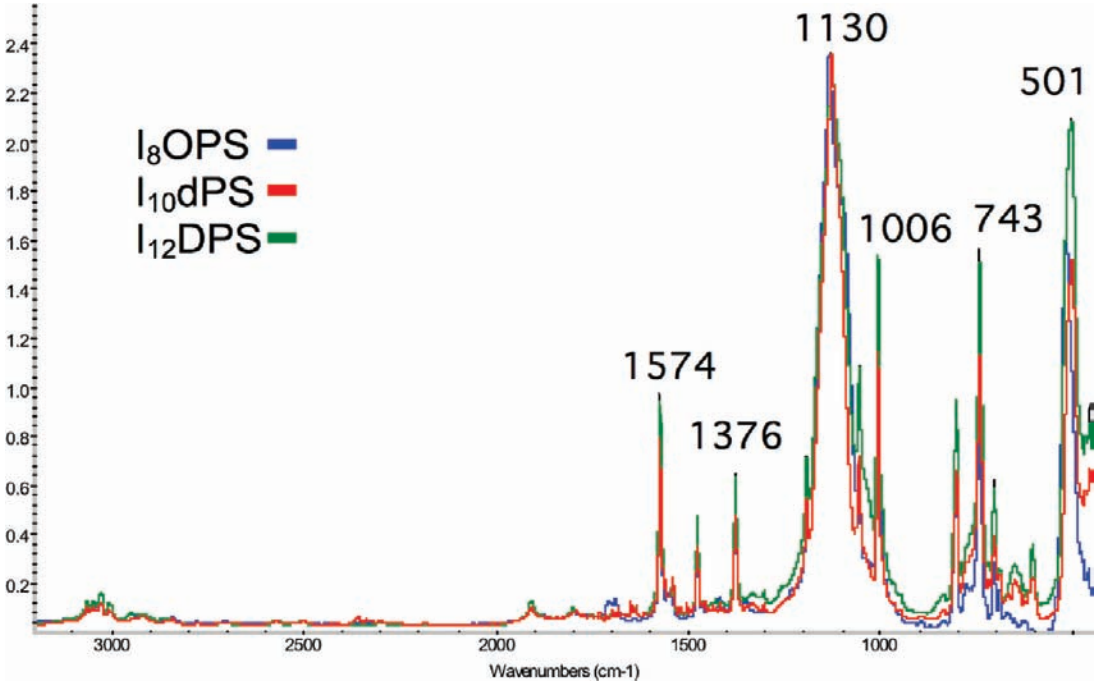

Figure 6. FTIR of the homologous iodophenylsilsesquioxanes at 3200−450 cm^{-1}. Legend colors correspond to each trace.

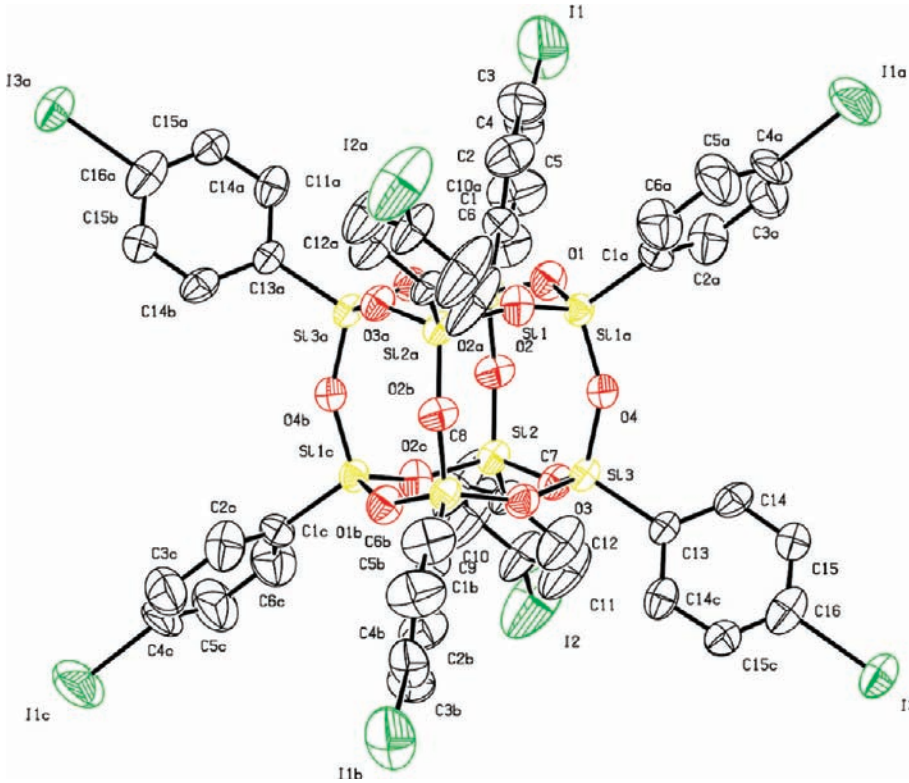

Figure 7. Thermal ellipsoid plot (50% probability) of $[p\text{-I-C}_6\text{H}_4\text{SiO}_{1.5}]_8$.[25] Hydrogen atoms are omitted for clarity. Full XRD data are given in ref 25.

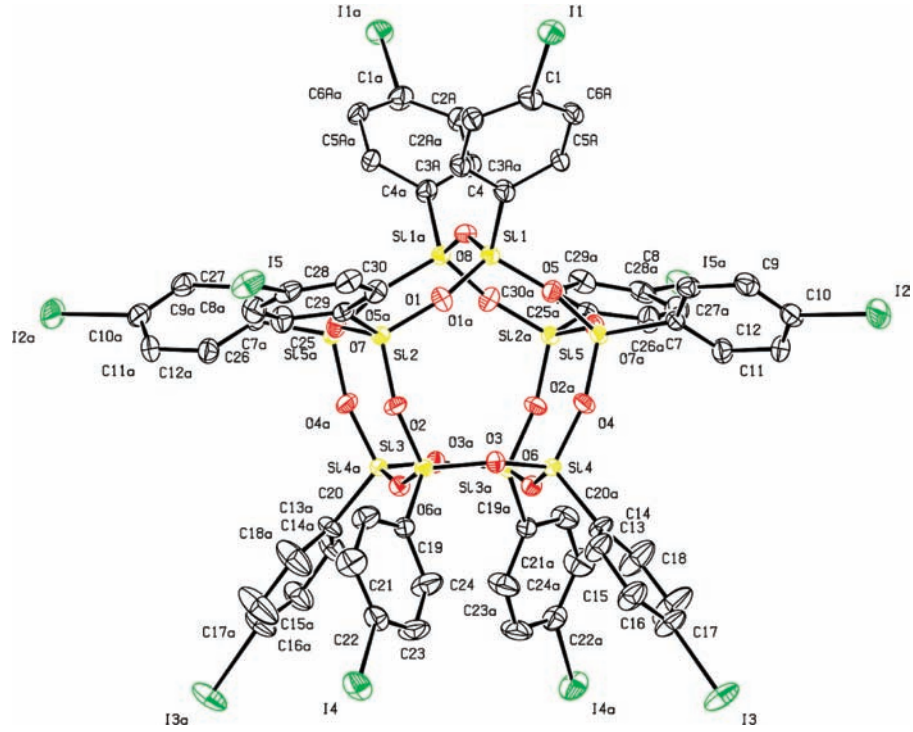

Figure 8. Thermal ellipsoid plot (50% probability level) of $[p\text{-I-C}_6\text{H}_4\text{SiO}_{1.5}]_{10}$. Hydrogen atoms are omitted for clarity. Full XRD data are given in the Supporting Information.

group *C*2/*c*. The unit cell contains four molecules with a total volume of 11 928 Å^3. Figure 9 shows the structural refinement. Two ordered *m*-xylene molecules cocrystallize with I_{12}DPS and are not shown.

Figures 7−9 demonstrate the different nano building block geometries available in this series of compounds. In each case the organic periphery points directly out from the center of the molecule, allowing for substitutions spaced symmetrically over

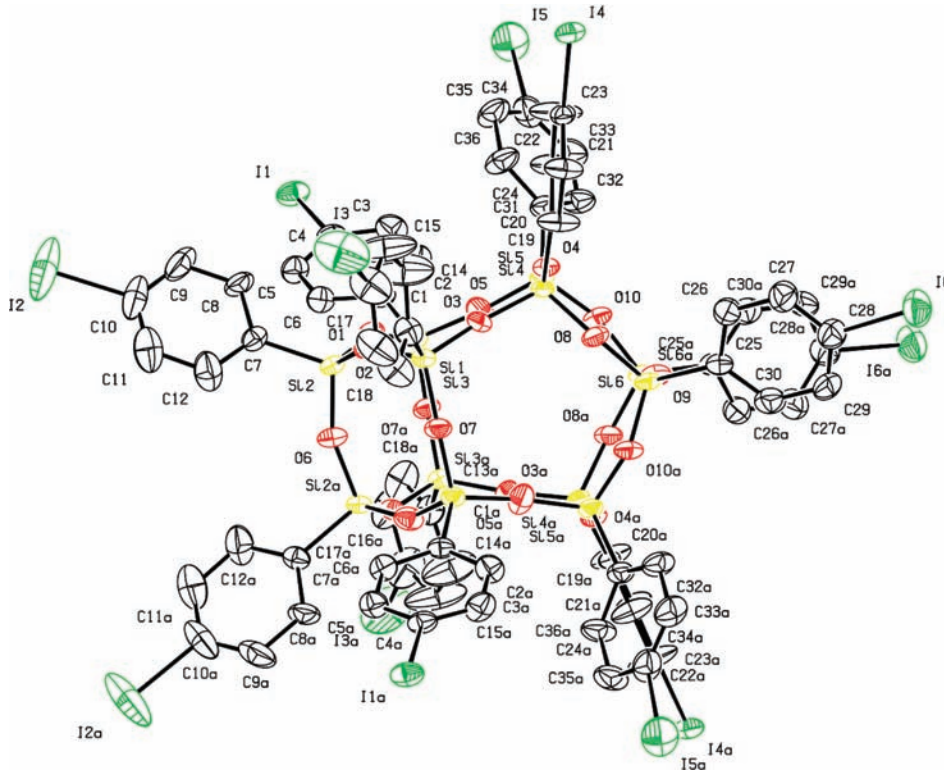

Figure 9. Thermal ellipsoid plot (50% probability level) of [*p*-I-$C_6H_4SiO_{1.5}$]$_{12}$. Hydrogen atoms and *m*-xylene solvates are omitted for clarity. Full XRD data are given in the Supporting Information.

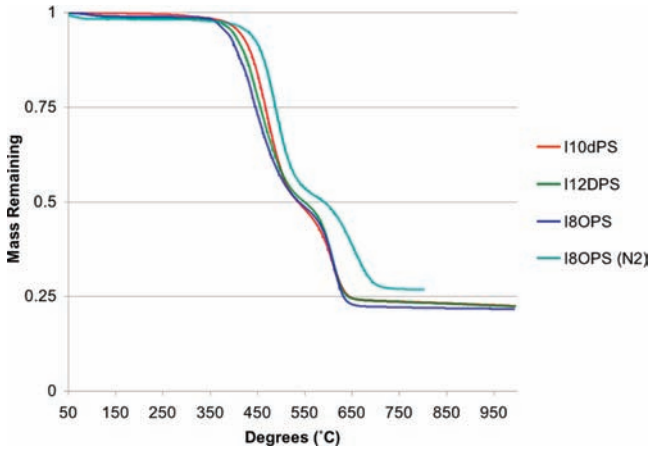

Figure 10. TGA of the series [*p*-I-$C_6H_4SiO_{1.5}$]$_{8/10/12}$.

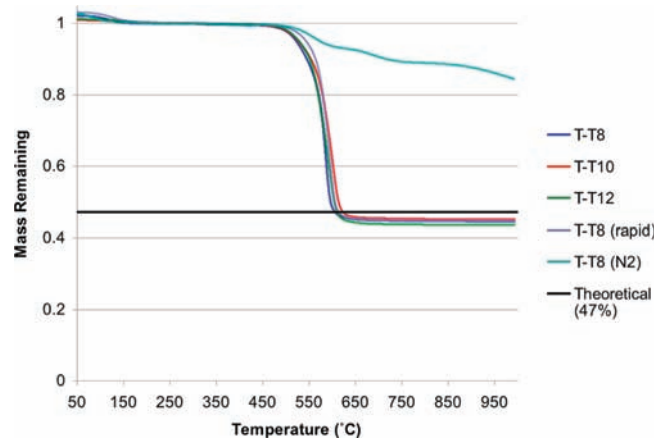

Figure 11. TGAs inair (10 °C/min) of T-I_8OPS, T-I_{10}dPS, and T-I_{12}DPS.

the exterior of the volume. This disposition ensures that each functional group is separated by a nearly equal distance over the entire molecular volume.

Synthesis and Physical Characterization of Thermally Cross-Linked Microporous Derivatives. The TGA (Figure 10) of these materials reveals consistent mass losses beginning at ~400 °C. The inflection in the TGA near 550 °C at ~50 wt % is consistent with the 49 wt % I in these compounds. Note that each compound cocrystallizes with solvent, which is removed easily under mild vacuum and as such is not seen in the TGA data.

Figure 11 records TGAs of samples of each compound previously heated to 450 °C and labeled as such as the thermolyzed cage: T-T_8, T-T_{10}, T-T_{12}, and T-T_8 (rapid). In these separate experiments, crystalline I_2 could be observed in the cooler sections of the thermolysis tube. These TGA traces were run in air with one also run in N_2. The evolution of I_2 must be accompanied by the generation of aryl radicals. These radicals are expected to recombine to form C−C bonds, producing covalently cross-linked solids.[70,71]

The thermolysis[72−75] and photolysis[75−77] of low-energy C−I aromatic bonds, generating I_2 and aryl radicals, have been

(69) (a) Spek, A. L. PLATON, A Multipurpose Crystallographic Tool; Utrecht University, Utrecht, The Netherlands, 2008. (b) Van der Sluis, P.; Spek, A. L. *Acta Crystallogr.* **1990**, *A46*, 194–201.
(70) Smith, D. W., Jr.; Shah, H. V.; Perera, K. P. U.; Perpall, M. W.; Babb, D. A.; Martin, S. J. *Adv. Funct. Mater.* **2007**, *17*, 1237–1246.
(71) Johnson, J. P.; Bringley, D. A.; Wilson, E. E.; Lewis, K. D.; Beck, L. W.; Matzger, A. J. *J. Am. Chem. Soc.* **2003**, *125*, 14708–14709.

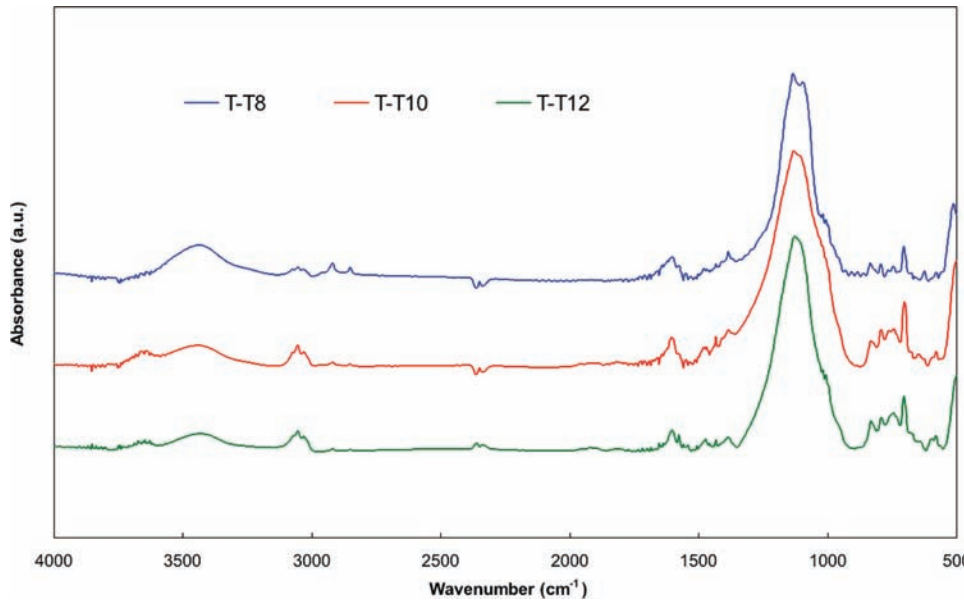

Figure 12. FTIR of T-T_8, T-T_{10}, and T-T_{12}. The ν(Si−O−Si) peak remains at ca. 1130 cm^{-1}.

studied extensively.[78–80] These radicals can be used to initiate other reactions or create new C−C bonds via recombination.[70,71,74,75,77] The high symmetry of the crystalline [*p*-I-$C_6H_4SiO_{1.5}$]$_{8/10/12}$ compounds coupled with the fact that the decomposition is stoichiometric in I_2 loss suggests that thermolysis could readily result in 3-D ordered structures that retain at least part of the initial crystal packing symmetry. In addition, these same materials might also serve as nano building blocks used to generate multiple radicals to create highly cross-linked materials for example for photonanolithography[81] or as UV curing agents. To our knowledge, no one has used this decomposition process to form microporous materials. Thus, the following results suggest considerable potential to access quite novel microporous materials using a variety of iodinated aromatic compounds.

At this point it is important to recall that the T_8 compound alone crystallizes in a tetragonal space group with $a = b = 20$ Å and $c = 21.5$ Å: nearly cubic with four molecules per unit cell. It may be reasonable to assume that this structure offers the desired nearly perfect packing that, if preserved in the thermolysis product, will produce grains that offer near-cubic symmetry.

The mass yields were calculated by measuring mass loss after thermolysis. For the thermolyzed samples T-T_8, T-T_{10}, T-T_{12}, and T-T_8 (rapid) (see the Experimental Section for processing details) these yields were 55%, 53%, 56%, and 52%, respectively, while the theoretical yield is 50.2%. The higher mass yield indicates that it is likely that water is readily absorbed from the atmosphere, and the presence of water is seen in the FTIR of these materials between 3500 and 3300 cm^{-1} (Figure 12).

After thermolysis T-T_8, T-T_{10}, T-T_{12}, and T-T_8 (rapid) each have a nominal composition of $O_{3/2}Si-C_6H_4-C_6H_4-SiO_{3/2}$. The TGAs of T-$T_{8/10/12}$ in Figure 11 give a 45 wt % ceramic yield, which is (within the error limits of the system) close to theory (47%). These TGAs also indicate no additional loss of iodine, as the mass loss begins at ~500 °C. TGA analysis under N_2 for T-T_8 gave a ceramic yield of 85% at 1000 °C. This implies that significant intermolecular cross-linking prevents facile cleavage of the remaining C−C and Si−C linkages. Further studies would be needed to demonstrate the structural effects of heating above 500 °C, but this could be a route to stable sacrificial coatings for high-temperature oxidative environments.

FTIR spectra of the N_2 thermolyzed products (Figure 12 and Figure S12 (Supporting Information)) are characterized by a strong ν(Si−O−Si) band at 1121−1129 cm^{-1} and the absence of ν(Si−O−Si) bands at 1045−1060 cm^{-1} that might be expected for disordered amorphous silica.[31] Note also the absence of a band at 920 cm^{-1} that would indicate the presence of ν(Si−OH). These findings suggest that the cage structures are retained during thermolysis.

The N_2 sorption isotherms (Figure 13) reveal type I behavior typical of microporous solids. With a pressure range of $5.00 \times 10^{-2} \leq P/P_0 \leq 3.00 \times 10^{-1}$, surface areas were calculated using the Langmuir method to be 830, 670, and 740 m^2/g (555, 455, and 500 m^2/g BET) and total pore volumes of 0.31, 0.26, and 0.27 cm^3/g for T-T_8, T-T_{10}, and T-T_{12}, respectively (Table 5).[82]

Pore size distribution analyses (Figure 14; see also Figures S13−S15 in the Supporting Information) of these products by

(72) Robaugh, D.; Tsang, W. *J. Phys. Chem.* **1986**, *90*, 5363–5367.
(73) Kumaran, S. S.; Su, M.-C.; Michael, J. V. *Chem. Phys. Lett.* **1997**, *269*, 99–106.
(74) Cho, H.-Y.; Ajaz, A.; Himali, D.; Waske, P. A.; Johnson, R. P. *J. Org. Chem.* **2009**, *74*, 4137–4142.
(75) Szulczewski, G. J.; White, J. M. *Surf. Sci.* **1998**, *399*, 305–315.
(76) Ajitha, D.; Fedorov, D. G.; Finley, J. P.; Hirao, K. *J. Chem. Phys.* **2002**, *117*, 7068–7076.
(77) Sharma, R. K.; Kharasch, N. *Angew. Chem., Int. Ed.* **1968**, *7*, 36–44.
(78) Zhang, X.; Friderichsen, A. V.; Nandi, S.; Ellison, G. B.; David, D. E.; McKinnon, J. T.; Lindeman, T. G.; Dayton, D. C.; Nimlos, M. R. *Rev. Sci. Instrum.* **2003**, *74*, 3077–3086.
(79) Friderichsen, A. V.; Radziszewski, J. G.; Nimlos, M. R.; Winter, P. R.; Dayton, D. C.; David, D. E.; Ellison, G. B. *J. Am. Chem. Soc.* **2001**, *123*, 1977–1988.
(80) Bunnett, J. F.; Wamser, C. C. *J. Am. Chem. Soc.* **1966**, *88*, 5534–5537.
(81) Pease, R. F.; Chou, S. Y. *Proc. IEEE* **2008**, *96*, 248–270.
(82) Sing, K. S. W.; Everett, D. H.; Haul, R. A. W.; Moscou, L.; Pierotti, R. A.; Rouquerol, J.; Siemieniewska, T. *Pure Appl. Chem.* **1985**, *57*, 603–619.

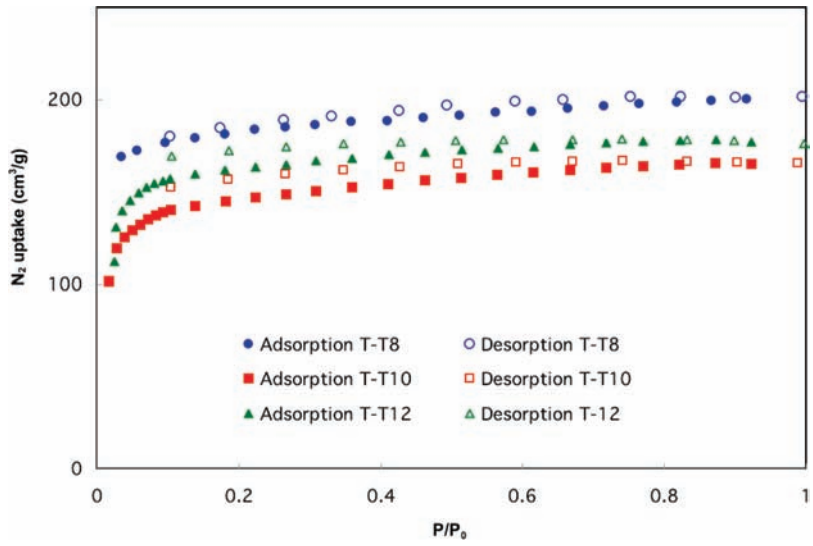

Figure 13. Nitrogen sorption isotherms of products at 77 K.

Table 5. Characterization Data for T-T_8, T-T_{10}, and T-T_{12}

		CY[a]		SA, m^2/g		
compd	mass yield, %	calcd	found	Langmuir	BET	pore vol, cm^3/g
T-T_8	55	47	45	830	555	0.31
T-T_8 (rapid)	53	47	45			
T-T_{12}	56	47	45	670	455	0.26
T-T_{10}	52	47	44	740	500	0.27

[a] CY = ceramic yield in air/10 °C/min.

NLDFT methods using Ar at 87 K show a narrow distribution of micropores of ≤10 Å.[82] These microporous networks may potentially be used as hybrid organic/inorganic molecular sieves for higher temperature separation processes.[83,84] These pore sizes are similar to those of larger pore zeolites such as NaX, and the combination of silica and organic surfaces is likely to change physisorption behaviors.[84] Water transport through ~1 nm hydrophobic pores has been cited as a one route to desalination and should be explored.[85]

While the reaction chemistry is presumably identical for each system, and the average pore structures and surface areas appear quite similar, powder XRD indicates that the T-T_8 materials have significantly more long-range order, as might be expected from their higher 3-D symmetry, as discussed above. In particular, the T-T_{12} and T-T_{10} materials show broad diffraction peaks at *d* spacings of ~25 Å, whereas the I_8OPS-derived materials show much narrower diffraction peaks at *d* spacings of 23, 20, and 18 Å (Figure 15).

The SEM images in Figures 16 and 17 reveal gross morphological differences between the systems. Images of T-I_{12}DPS in Figure 16 (Figures S16−S20 in the Supporting Information) show conchoidal fracture (also in T-T_{10}), indicating a disordered, glassy structure. In contrast, T-T_8 materials show striated fracture surfaces reminiscent of exfoliation or fracture of lamellar structures (Figure S20), implying a much more significant underlying connectivity.

Of potential value to our above arguments, Figure 17 (top right) shows a microstructure that suggests cubic/rectangular grains within a lamellar type of supramacromolecular structure. These features appear to support our proposal that the original packing of the unit cells is translated through to the global structure and accounts for the higher crystallinity observed in the XRD as well as the higher surface areas observed in the T-T_8 product.

Conclusions

The results reported here provide a method of preparing highly symmetrical para-iodinated T_8, T_{10}, and T_{12} phenylsilsesquioxanes which, on the basis of the extensive literature on catalytic cross-coupling reactions, should allow the development of highly symmetrical molecules and 3-D structures from them that offers considerable potential to compare structure−property relationships in sets of molecules and materials in 3-D heretofore impossible.

Coincidentally we developed an improved route to the T_{10} decaphenylsilsesquioxane. In particular, I_8OPS can be synthesized in 100 g quantities with >90% yields and, following careful recrystallization, to ≥95% selectivity for para substitution. I_{10}dPS was isolated in small but useful quantities, and I_{12}DPS was produced at the 25 g scale. Each of these compounds offers nearly equivalent chemical reactivity with very different geometries.

The crystal structures of these three compounds were determined, and an analysis of the differing motifs in supermolecular coordination will be undertaken in future publications.[86] These compounds offer a variety of symmetries and allow the addition of diverse functional groups. The high degree of symmetry, coupled with the ability to tailor the functionality of the periphery, suggest that these molecules will also offer the potential to create a 3-D network.

Finally, we have been able to demonstrate the use of thermal dehalocoupling as a means to produce unique microporous solids with microstructures that seem to derive from the initial molecular packing of the starting iodides. We have demon-

(83) Dinca, M.; Long, J. R. *J. Am. Chem. Soc.* **2005**, *127*, 9376–9377.
(84) Davis, M. E.; Lobo, R. F. *Chem. Mater.* **1992**, *4*, 756–768.
(85) Shannon, M. A.; Bohn, P. W.; Elimelech, M.; Georgiadis, J. G.; Marinas, B. J.; Mayes, A. M. *Nature* **2008**, *452*, 301–310.
(86) Roll, M. F. Ph.D. Dissertation, University of Michigan, 2010.

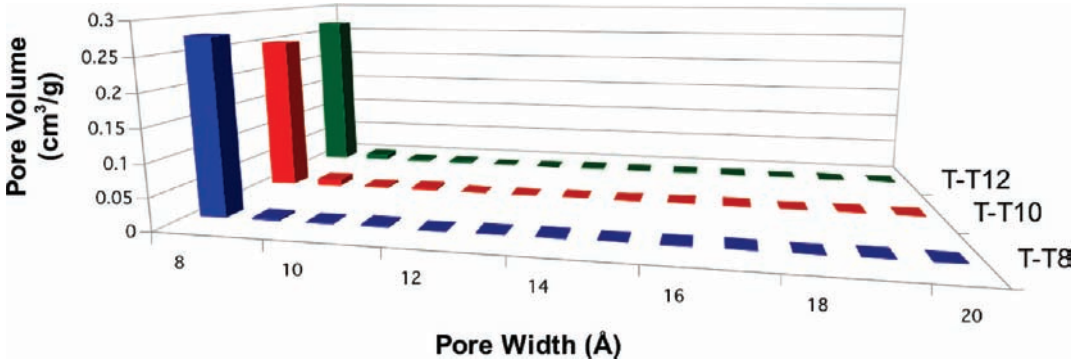

Figure 14. Pore size distribution data of T-I_8OPS, T-I_{10}dPS, and T-I_{12}DPS.

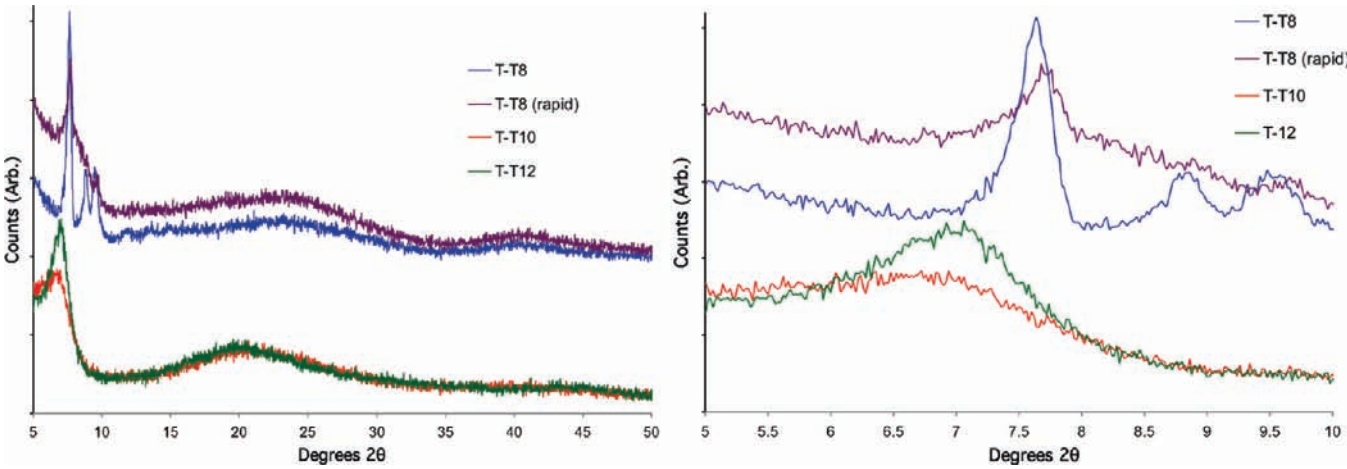

Figure 15. XRD powder patterns of T-T_8, T-T_{10}, and T-T_{12}: (a) full scale; (b) expanded scale.

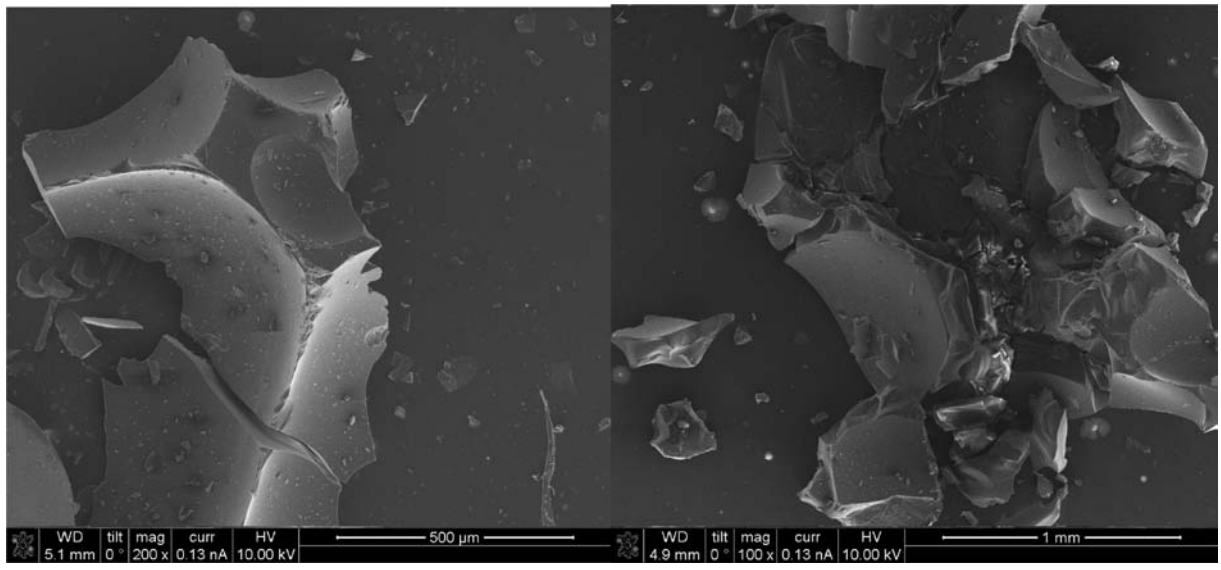

Figure 16. SEM of T-T_{12} and T-T_{10} showing evidence of conchoidal fracture typical of glassy materials. See also Figures S18 and S19 in the Supporting Information.

strated, for the first time, the synthesis of network solids with specific surface areas of 500−700 m^2/g and average pore sizes <1 nm.

Critically, we have demonstrated a route to produce network solids with identical chemistries starting from three different high-symmetry, high-functionality, crystalline hybrid nano building blocks[10] as precursors. There are discernible differences in the macroscopic structures of the final products, a step toward the goal of designing organic/inorganic nanocomposites with completely tailored properties, from the nanometer length scale up. The use of these materials for surface modification of other structures by radical or other

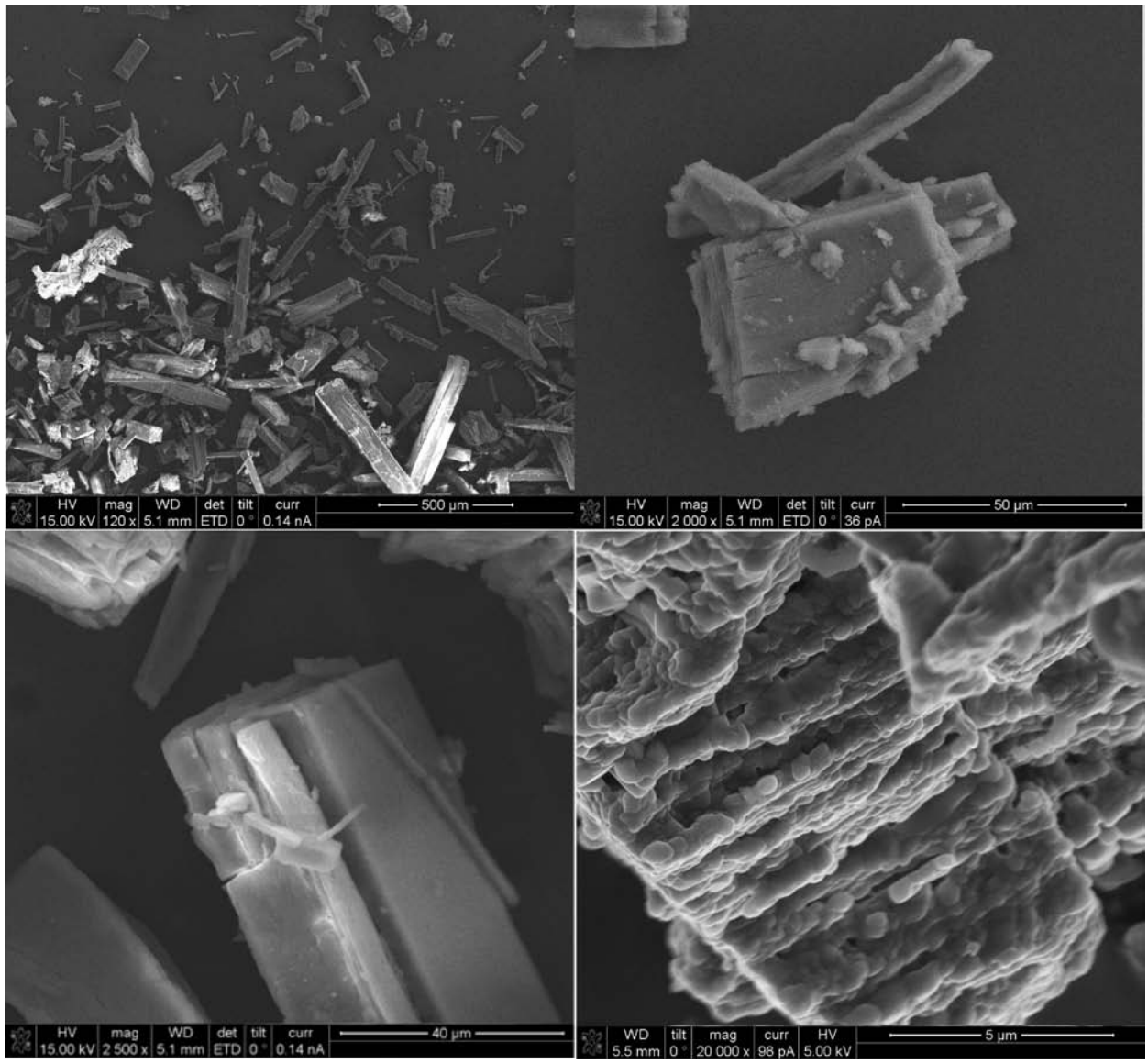

Figure 17. SEMs of T-T_8, suggesting retention of the original crystal morphology. See also the Supporting Information.

chemistries should also be explored. Future publications will address these possibilities.

Acknowledgment. We thank the NSF for support of this work through Grant No. CGE 0740108. We wish to acknowledge the assistance and counsel of Prof. Adam J. Matzger and Dr. K. Koh throughout this project and give special thanks to Santy Sulaiman for the use of an IR spectrum and J. Jokisaari for the SEM micrographs.

Supporting Information Available: CIF files giving crystallographic data and figures giving ^{1}H and ^{13}C NMR and FTIR spectra, TGA plots, adsorption/desorption isotherms, powder X-ray diffraction patterns, and SEM micrographs. This material is available free of charge via the Internet at http://pubs.acs.org.

JA102453S